An Overview of THz Research Activities in Taiwan

Ci-Ling Pan

Department of Photonics and Institute of Electro-Optic Engineering
National Chiao Tung University 1001 Ta-Hsueh Rd., Hsinchu, Taiwan 30010, R.O.C.
Contact: clpan@faculty.nctu.edu.tw

ABSTRACT

Reflecting the flourishing THz science and technology in the past decade, a number of groups in Taiwan have initiated research activities in this area. All major research universities as well as the semi-public Industrial Technology Research Institute are represented. Current research topics include THz devices (emitters, detectors, phase shifters) and the applications of THz time-domain spectroscopy to the study the far-infrared optical properties of various materials. Highlights of recent research activities are outlined.

Keywords: THz, transmitters, emitters and detectors, phase shifters, optics, phase shifters, photonic crystals

INTRODUCTION

Terahertz (THz) wave, the electromagnetic radiation in a frequency interval from 0.1 to 10 THz, occupies a large portion of the electromagnetic spectrum between the infrared and microwa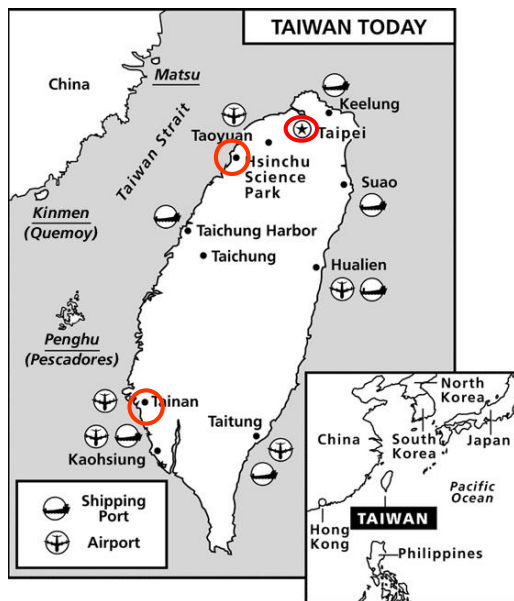ve bands. THz wave is also referred to as sub-millimeter wave or far-infrared (FIR) radiation. In the past decade, sub-millimeter wave or terahertz (THz) technology[1] has undergone remarkable growth with intense interests for their applications in time-domain far-infrared spectroscopy,[2,3] imaging,[4] ranging[5] and bio-medical applications.[6] Reflecting the flourishing THz science and technology in the past decade, a number of groups in Taiwan have initiated research activities in this area. All major research universities as well as the semi-public Industrial Technology Research Institute are represented. Current research topics include THz devices (emitters, detectors, phase shifters) and the applications of THz time-domain spectroscopy and imaging to the study the far-infrared optical properties of various materials as well as topics of interests in biomedicine. In this paper, we present highlights of recent THz research activities in Taiwan.

Fig.1 A map of Taiwan with location of major THz research activities.

Figure 1 shows a map of Taiwan and the cities in which the THz research groups are located. From north to the south, in the capital city of Taipei, Professor Chi-Kuang Sun's group at National Taiwan University (NTU) is located. About 80 km south of Taipei, Hsinchu city boasts National Tsing-Hua and Chiao Tung Universities (NTHU and NCTU), the Industrial Technology Research Institute (ITRI) and the world-famous Hsinchu Science Park. THz research groups of Profs. C. C. Chi, S. F. Hong, and Y. C. Huang are affiliated with NTHU. Profs. C. S. Chang, K. H. Wu, C. P. Lee, S. T. Yen, Ru-Pin Chao Pan and myself are with NCTU. ITRI, in collaboration with my group, has recently initiated programs in THz studies of biomedicine and frequency metrology. Further south, about three hundred km south of Taipei, lays National Cheng-Kung University (NCKU) and Prof. C. H. Huang's group. It is not possible for me to grasp fully the scope of research activities of my distinguished colleagues. I will attempt to briefly review some of the highlights, mainly those from my own group.

EDGE-COUPLED MEMBRANE THZ TRANSMITTERS
BASED ON A THZ-BANDWIDTH MSM TWPD

The NTU team recently proposed and demonstrated a TWPD with world record 570 GHz electrical band width. The quantum efficiency of the TWPD was high as 8% (λ = 800 nm). Based on this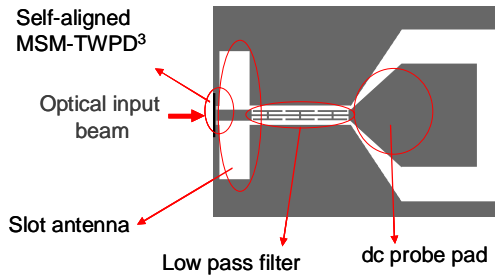, an edge-coupled membrane THz transmitter was developed[7,8] The device is based on LTG-GaAs and an external light-THz conversion efficiency of at a 1.6-THz radiation frequency was achieved. Figure 1 shows the structure of the new membrane photonic transmitter, which is composed of a high-speed photodetector, a radio frequency (RF) choke filter, and a planar antenna. The photodector was previously reported metal–semiconductor–metal traveling-wave photodetector (MSM-TWPD)[7] and a coplanar-waveguide-fed slot antennas was adopted due to its easy connection with planar devices and higher radiation power than the spiral antennas at the resonant frequency. The absorption length of the TWPD employed in the photonic transmitter is 50 m while the center strip and air gap widths are 2 and 0.3 m, respectively. The RF choke filter, which acts as an inductance , avoids the high frequency ac current (with a resonant frequency of the slot antenna) leaking into the dc probe pad that will lower the radiation efficiency. As an example, consider a device fabricated on a LTG-GaAs layer on top of an AlGaAs cladding layer with antenna resonating at 650 GHz. The GaAs substrate was removed to form a membrane structure whose total thickness is 5 m. The membrane device was then mounted on a glass substrate. The measured frequency response of the photonic transmitter is shown in Fig. 3(a). Operating at its antenna's resonant frequency of 645 GHz, the measured external conversion efficiency (including the coupling loss into the TWPD, the loss in the glass substrate, and loss in the collection system) versus applied bias voltages under 0.93-mW average-power optical excitation is shown in Fig. 3(b). The conversion efficiency of the device increases with increased bias and starts to show some saturation behavior if the bias is higher than 8 V. The saturation behaviors determine the optimum device operation condition, which was influenced by detector bias and optical excitation power at the same time. By considering these two factors together, we have successfully uncovered the optimum operation condition for photonic transmitter and a maximum external light-THz conversion efficiency of 0.11% was achieved with 645-GHz radiation.[9] With such a high conversion efficiency of the edge-coupled membrane structures, a compact THz source integrated with semiconductor lasers is possible to be realized.

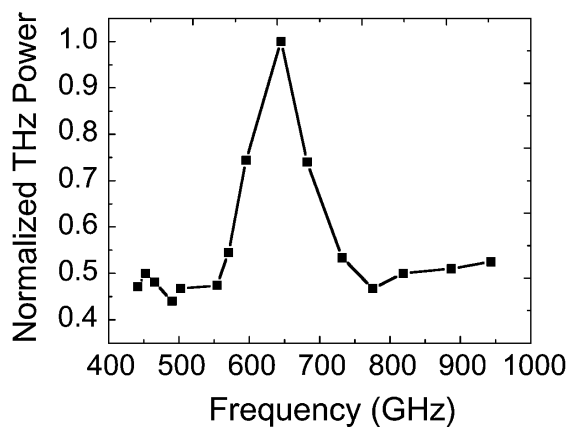Fig.2 Structure of the edge-coupled membrane photonic transmitter.

Fig.3(a) Measured frequency response of the photonic transmitter with an antenna resonating at ~650 GHz.
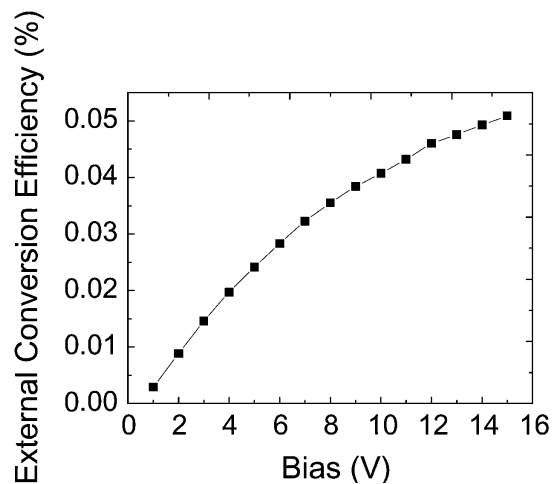
Fig.3(b) External conversion efficiency of the photonic transmitter versus detector bias under 0.93-mW optical excitation.

WAVEGUIDE-ENHANCED THZ PARAMETRIC GENERATION AND OSCILLATION IN THIN LITHIUM NIOBATE WAFERS

This is the work of Prof. Y. C. Huang's group at NTHU. There are a number of ways for generating coherent tera-hertz (THz) wave radiations. For high-power coherent THz radiations, free-electron laser has been the method of choice. For low-power coherent THz radiations, nonlinear frequency mixing provides a relatively compact and economic alternative to a free-electron laser. To date, most THz nonlinear frequency mixing processes done in lithium niobate employed a non-collinear phase-matching configuration, where a Nd:YAG pump laser is polarized along the crystallographic z direction and a THz radiation is generated at a ~ 65° angle from the pump laser. This non-collinear phase matching scheme is useful for separating the THz wave from the other mixing waves, but severely limits the parametric gain length and attenuates the THz wave in lithium niobate. Waveguide confinement is known to enhance the efficiency in a nonlinear frequency mixing process. In this paper, we take advantage of mode confinement in a lithium niobate waveguide and demonstrate efficient THz parametric generation with a relatively low pump power at 1064 nm.

Figure 4 shows the schematic of the experimental setup. The pump source is an actively Q-switched Nd:YAG laser (Minilase II, New Wave), producing 20-Hz, 6-ns pulses at 1064 nm. The THz parametric gain medium was a 45-mm long z-cut congruent lithium niobate wafer. The thickness of the lithium niobate wafer was varied from 500, 780, to 1000 μm during experiment. With an output wavelength of a few hundred microns, the lithium niobate wafer is a planar waveguide at THz. To couple out the non-collinear phase matched THz wave, we cut one corner of the lithium niobate wafer so that the THz output emits to the normal direction of the crystal cutting edge. The pump wave is removed downward from the successive total internal reflections inside the lithium niobate crystal. Along the signal path, the end surfaces of the lithium niobate were coated with anti-reflection dielectric layers at the signal
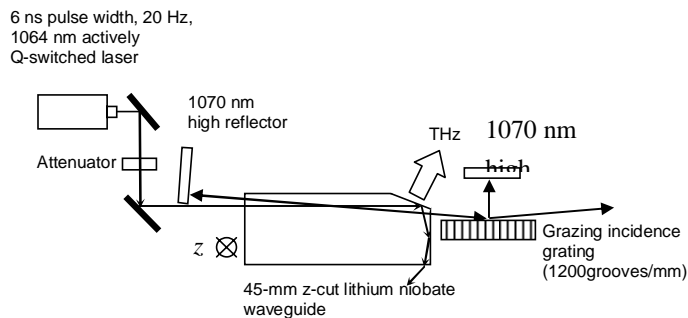

Fig.4 The schematic of the narrow-line THz waveguide parametric oscillator with an intracavity grazing-incidence grating. Without the high reflectors and the grating, the configuration is a THz parametric generator.

wavelength. With the 1070-nm high reflectors, the setup in Fig. 4 is a THz parametric oscillator (TPO) with an intracavity grazing-incidence grating. The intracavity grating has a ruling of 1200 lines/mm. Without the two high reflectors and the intracavity grating, the device in Fig. 3 is a THz parametric generator (TPG).

Table 1 shows the measured signal's output characteristics for the three crystal thicknesses under the same pump intensity of 209 MW/cm². During the experiment, the pump energy was kept at 2 mJ/pulse and the pump beam size remained unchanged. It is evident from Table 1 that the pump-to-signal conversion efficiency was increased by more than a factor of two when the thickness of the lithium niobate wafer was reduced from 1 mm to 500 μm. Also, the signal pulse width was correspondingly reduced from 4 ns to 2.8 ns. The reduction in the signal pulse width is a signature of high-gain parametric generation due to a highly nonlinear growth rate of the signal wave in an exponential-gain process. Since the pump and measurement configurations were the same for all three lithium niobate samples of different thickness, the efficiency enhancement in a thin lithium niobate is attributed to waveguide confinement. The 1.61% parametric conversion from the 500 μm thick TPG, to the best of our knowledge, is the highest from a 1064-nm pumped lithium niobate TPG at a pump energy of 2 mJ/pulse.

Table 1 Signal's output characteristics from 500, 780, and 1000 μm thick lithium niobate wafers under a pump intensity of 209 MW/cm² and a pump energy of 2 mJ/pulse.

Crystal thickness	Signal pulse width	Signal output energy	Conversion efficiency
500 μm	2.8 ns	32.8 μJ	1.61%
780 μm	3.2 ns	26.6 μJ	1.31%
1000 μm	4.0 ns	15 μJ	0.75%

The novel configuration of the TPO in Fig. 4 is expected to produce transform-limited, wavelength-tunable THz radiation with just one single-frequency pump source. Such a single-frequency pump can be an injection-seeded Q-switched Nd:YAG laser. The authors estimated a linewidth of 20 GHz at 3 THz for a grating angle of 88°. To measure the THz output wavelength, the authors used a room-temperature deuterated triglycine sulfate (DTGS) pyrodetector immediately after a variable-gap GaAs etalon near the output edge of the lithium niobate crystal.   Each of the two GaAs etalon plates has a thickness of 0.633 mm. Figure 5 shows the result of the etalon scan at a pump energy of 2 mJ/pulse. The characteristic period in Fig. 3 indicates a THz wavelength of 162 µm.   A typical DTGS pyrodetector has a detection limit of sub-nJ at THz. Estimated from the signal-to-noise ratio in Fig. 3, several nJ/pulse THz energy was generated from the TPO, which is consistent with the tens of µJ signal energy from the TPG listed in Table 1.
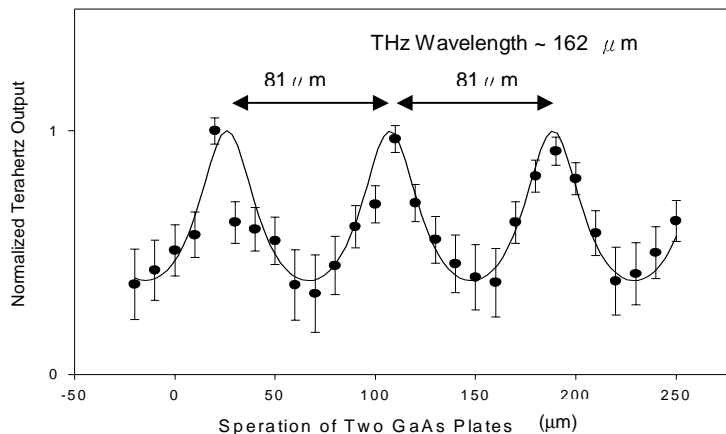

Figure 5. The THz intensity from the grating TPO measured by a GaAs scanning etalon. The characteristic period indicates a THz wavelength of 162 µm.

NCTU THZ PHOTONICS PROGRAMS

There are several faculty with research interests in THz science and technology.   Prof. K. H. Wu of the Electrophysics Department is interested in Generation of THz Radiation and Its Application in the Studies of Electrodynamics of High-Tc Superconductors in THz Regime.   The group of Profs. C. P. Lee and S. T. Yen are working on The generation of THz radiation from uniaxially strained B-doped Ge lasers. High-quality GaSe crystals are grown in Prof. C. S. Chang's laboratory.   Tunable MIR radiation up to 39 µm has been achieved in these crystals through difference frequency generation process.

Following is a summary of THz studies made by my group and collaborators in the past five years: We have reported characteristics of optically excited THz radiation from arsenic-ion-implanted GaAs (GaAs:As$^+$)[10] and multi-energy proton-bombarded GaAs.[11] Dipole and medium-gap THz photoconductive antennas based on arsenic-ion-implanted GaAs (GaAs:As$^+$) were shown to be effective THz emitters. [12,13]   Record-high detection bandwidth of 30 THz was realized with GaAs:As$^+$ and InP:H$^+$ dipole antennas.[14,15]   The GaAs:As$^+$ substrate was prepared by implanting the semi-insulating (SI) GaAs substrate with arsenic ions at a total doses of 10^{16} ions/cm^2 with multiple energies of 50keV, 100keV and 200keV.   This was followed by furnace annealing at 600 °C for 30 minutes.   The ion implantation depth was estimated to be about 100 nm by SIMS (Secondary Ion Mass Spectroscopy) measurement.   Four InP: H$^+$ PC antennas were prepared by bombarding (100)-oriented SI-InP substrates with 180 keV proton with dosages of 1×10^{15}, 3×10^{15}, 1×10^{16} and 3×10^{16} ions/cm^2, respectively.   The LT-GaAs sample used as the reference was grown at a substrate temperature of 250 °C by molecular beam epitaxy and annealed at 600 °C for 5 min after growth.   The carrier lifetime of GaAs:As$^+$ samples were estimated to be around 1~2 ps by a transient photo-reflectance measurement (see Fig. 2). The carrier lifetimes of all InP: H$^+$ and LT-GaAs samples used in this experiment were also found to be shorter than 2 ps.   A micro-stripline dipole antenna was fabricated on each InP:H$^+$ wafer by standard cleaning, metallization and lift-off procedures for InP.   During the metallization processes, Ni-Ge-Au-Ge-Ni-Au metal layers were evaporated and

annealed at around 400°C. The antenna consisted of 5-μm-wide coplanar striplines (6-mm long) separated by 20-μm and contacts, rectangular in shape, at the center of the coplanar striplines. The contact width and length (in vertical direction to the striplines) were 10 μm and 7.5 μm, respectively. The PC gap between the contacts was 5 μm.

Figure 6 shows the signal waveforms detected by the (a) GaAs: As^+, (b) SI- GaAs and (c) LT-GaAs PC antennas for THz radiation generated from the ZnTe emitter. THz waveform detected with the SI-GaAs antenna was averaged for three sequential scanning of the delay stage with a lock-in amplifier constant of 0.3 sec, while for the other PC antennas the scanning was only once. The detected peak signal current from GaAs:As^+, SI GaAs and LT-GaAs PC antennas was 0.02 nA,0.3 nA and 0.24 nA, respectively. The signal to noise ratio (SNR) was estimated to be about 20, <10 and 100, respectively. The signal current detected with the GaAs: As^+ PC antenna was lower than the other two types PC antennas by one order, while the noise level was comparable to that with the LT-GaAs PC antenna. The low signal in the GaAs: As^+ PC antenna is attributed to the insufficient thickness of the arsenic ion-implanted layer, which was only 10% of the absorption depth (~ 1μm) at the excitation laser wavelength; Most of the carriers excited in SI-GaAs substrate beneath the ion-implanted layer could not contribute to the signal since after the photoconductive decay in As^+-ion-implanted layer, the long-lived carriers in non-ion-implanted SI-GaAs are blocked to flow into the antenna contact by the insulating layer. The SNR of SI-GaAs PC antenna was lowest, although the signal current level was the highest. The low SNR of SI-GaAs PC antenna is attributed to the large current noise originating from the long-lived photo-exited carriers (lifetime > 100 ps), while the other two have carrier lifetimes of 1~2 ps.

Figure 7 shows Fourier transformed amplitude spectra of the THz waveforms shown in Fig. 6. The spectral profiles are almost the same for the three cases. The high frequency end of the spectral distribution is extending to about 30 THz. The end of the spectral distribution above the noise floor was estimated to be 32 THz and 24THz for GaAs:As^+ and SI-GaAs PC antenna, respectively (40 THz for LT-GaAs PC antenna), which are the highest frequencies reported so far for the same kind of PC antennas. The spectral bandwidth was limited by the cut off frequency (~40 THz) due to the phase-mismatch between the THz radiation and pump laser pulse in the 10-um thick ZnTe emitter.
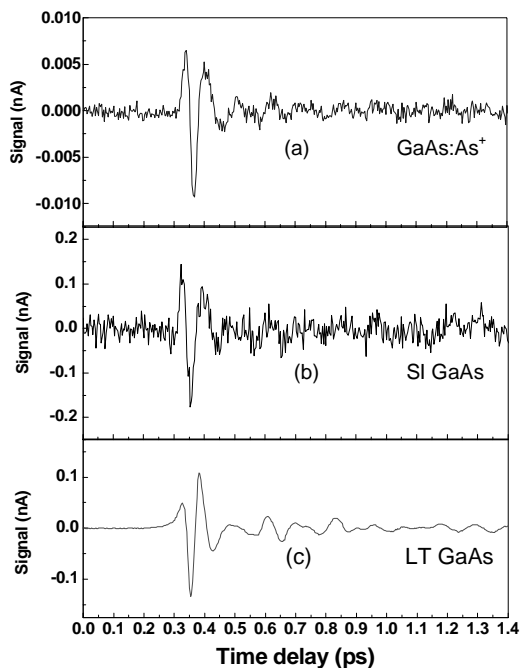

Fig.6 Time-resolved THz radiation waveforms detected by PC antenna based on (a) GaAs:As^+ ,(b) SI-GaAs and (C) LT-GaAs. The emitter was a 10-μm thick (110) ZnTe crystal.
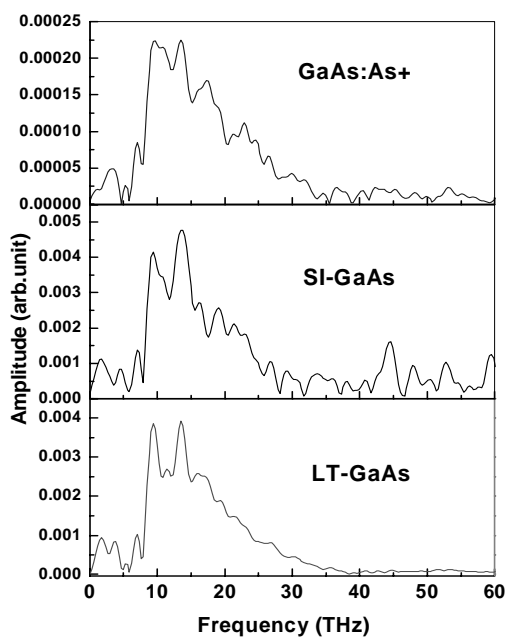
Fig.7 Fourier transformed amplitude spectra of the PC-detected THz waveforms shown in Fig. 4.

Although the SNR with GaAs:As[+] photoconductive (PC) antenna was lower than that of LT-GaAs PC antenna, it is possible to improve the efficiency by increasing the ion-implanted layer thickness. The peak THz signal of the InP:H^{+} (10^{15} ions/cm^2) PC antenna is slightly higher than that of the LT-GaAs one, while the SNR of the former is about half as high as the latter. This can be improved by increasing the resistivity of InP:H^{+} through optimizing the ion dosage level and/or the annealing condition. Our results indicate both GaAs:As[+] and InP: H^{+}, and other ion-implanted III-V photocoudctors could be developed into promising materials as the photoconductive substrate for ultrabroadband PC antennas.

We have also made progress in efficient intra-cavity THz generation.[16,17] Generation of narrow-band CW THz radiation was demonstrated by using a proprietary tunable dual-wavelength laser.[18] The coherence length of CW THz wave generated in this manner exceeds 100 cm, as determined by a home-made Martin-Pauplet Polarizing Interferometer. Together with Prof. Ru-Pin Chao Pan's group, we have began exploring the use of liquid crystal for THz optics. The large birefringence of liquid crystals (LCs) is well known and has been employed successfully for phase shifting of microwave and millimeter wave signals previously. The optical constants of several important liquid crystals were determined in the THz regime for the first time by using THz time-domain spectroscopy (THz-TDS).[19, 20] An electrically controlled room temperature THz phase shifter with 5CB has also been demonstrated.[21] A maximum phase shift of 4.07 was shown at 1.07 THz. The high voltage (~ 177V) was required. By using magnetically controlled birefringence in a 5CB cell with nominal thickness of 1.5 mm, we were able to achieve a maximum phase shift of 141° at 1.025 THz.[22] The alignment of the LC layer becomes increasingly difficult with thicker cells. Phase shift exceeding 360° at 1 THz, an important milestone, was realized by using a sandwiched LC (E7, Merck) cell as thick as 3 mm.[23]
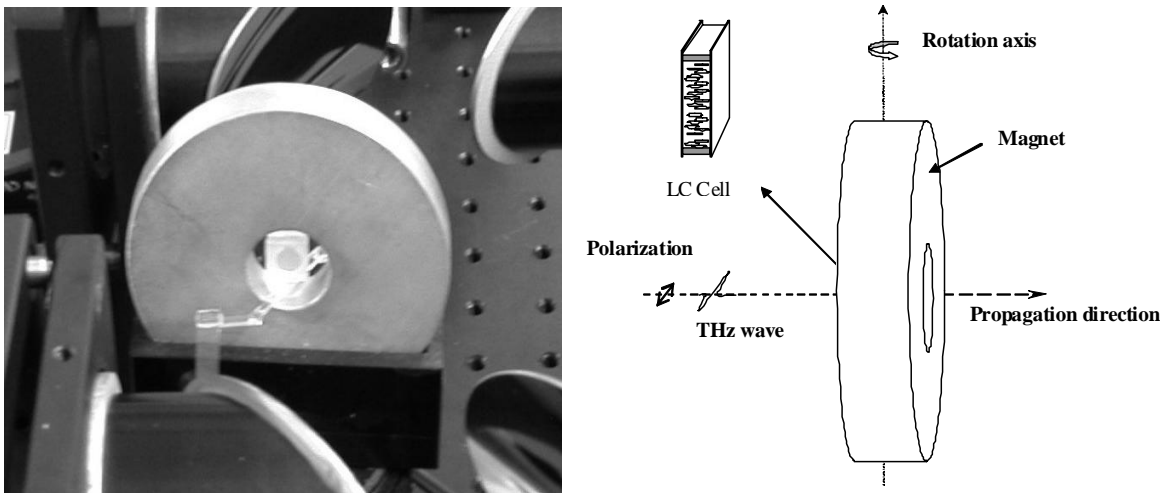

Fig.8 A photograph and the schematic diagram of the LC THz phase shifter..

The tunable THz Phase shifter consists of a homeotropically aligned LC cell and a rotary magnet as shown in Fig. 8. The magnetic inclination angle, θ, is defined as the angle between the magnetic field and the propagation direction. We can assume that the LC molecules are reoriented parallel to the magnetic field when the magnetic field is large enough as in this work [10] . The phase shift, δ(θ), due to magnetically controlled birefringence is given by

$$\delta(\theta) = 2\pi L \frac{f}{c} \left\{ \left[\frac{\cos^2(\theta)}{n_o^2} + \frac{\sin^2(\theta)}{n_e^2} \right]^{-\frac{1}{2}} - n_o \right\} \quad , \tag{1}$$

where n_o and n_e are the ordinary and extra-ordinary refractive indices of the LC, L is the thickness of LC layer, f is the frequency of the THz waves and c is the speed of light in vacuum.

Three fused silica plates are employed for the sandwiched cell. The two compartments of the cell are filled with a common LC, E7 (Merck0. Teflon spacers are used for controlling the thickness of LC layers to 1.5 mm each. The alignment of the LC molecules is homeotropic [10]. We employ an Nd-Fe-B sintered magnet on a rotation stage, which provides a tunable magnetic field for tuning the phase shift of the THz wave.

We use THz-TDS method for characterizing the device. We have also measured the extraordinary and ordinary refractive indices of E7, n_e and n_o in the THz frequency range.

In the 0.2-1.2 THz range, n_e varies from 1.69 to 1.80, while n_o varies from 1.51 to 1.63 for E7 at room temperature (25°C). The birefringence of E7 is thus 0.12 to 0.21 for the same frequency range. The corresponding imaginary indices of E7 are relatively small (< 0.04). The deduced phase shifts of the phase shifters are plotted as a function of the magnetic inclination angle in Fig. 2 for 0.49 and 1.025 THz waves. The maximum phase shift achieved was 368° at 1.025 THz and $\theta = 54^{\circ}$. The theoretical predictions are plotted as the solid curves in Fig. 9. They show good agreements with the measured results.
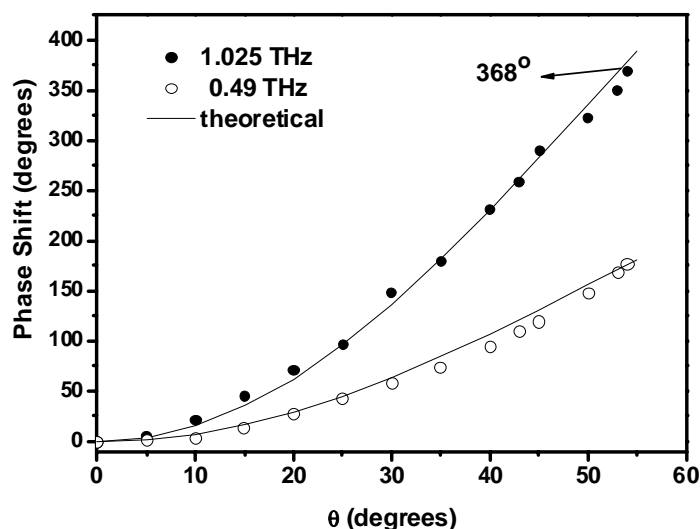

Fig. 9 The phase shift of the THz waves versus the magnetic inclination angle. The solid curves are theoretical predictions. The open and solid circles are experimentally measured phase shift at 0.49 and 1.025 THz.

SUMMARY

Reflecting the flourishing THz science and technology in the past decade, a number of groups in Taiwan have initiated research activities in this area. All major research universities, e.g., NTU, NTHU, NCTU as well as the semi-public Industrial Technology Research Institute (ITRI) are represented. Current research topics include THz devices (emitters, detectors, phase shifters) and the applications of THz time-domain spectroscopy to the study the far-infrared optical properties of various materials. Highlights of recent research activities are outlined.

ACKNOWLEDGEMENTS

REFERENCES

1.   P. H. Siegel, IEEE Trans. Microwave Theory Tech. **50**, 910 (2002).
2.   M. V. Exter, C. Fattinger, and D. Grischkowsky, Opt. Lett. **14**, 1128 (1989).
3.   D. Grischkowsky, S. R. Keiding, M. V. Exter, and C. Fattinger, J. Opt. Soc. Am. B **7**, 2006 (1990).
4.   B. B. Hu and M. C. Nuss, Opt. Lett. **20**, 1716 (1995).

5.   R. A. Cheville and D. Grischkowsky, Appl. Phys. Lett. **67**, 1960 (1995).
6.   A. J. Fitzgerald, E. Berry, N. N. Zinovev, G. C. Walker, M. A. Smith, and J. M. Chamberlain, Physics in Medicine and biology **47**, R67 (2002).
7.   J.-W. Shi, S.-W. Chu, M.-C. Tien, C.-K. Sun, Y.-J. Chiu, and J. E. Bowers, *Appl. Phys. Lett.* **81**, 5108 (2002).
8.   J.-W. Shi, K.-G. Gan, Y.-J. Yang, Y.-H. Chen, C.-K. Sun, Y.-J. Yang, and J. E. Bowers, *IEEE Photonic Technology Letters* **14**, 1587 (2002).
9.   M.-C. Tien, H. –H. Chang, J. –Y. Lu, L.-J. Chen, S.-Y. Chen, R. –B. Wu, W. -S. Liu, J. –I. Chyi, and C. –K. Sun,, *IEEE Photonic Technology Letters* **16**, 873 (2004) .
10.   G. R. Lin and C.-L. Pan, *Appl. Phys.* B**72**, 151 (2001).
11.   G. R. Lin and C. –L. Pan, Opt. Quantum Electron. **32**, 553 (2000).
12.   Tze-An Liu, Masahiko Tani, Gong-Ru Lin and Ci-Ling Pan, Proc. SPIE **4490**, 96 (2001).
13.   Tze-An Liu, Masahiko Tani, and Ci-Ling Pan , J. Appl. Phys. **93**, 2996 (2003).
14.   T. A. Liu, M. Tani, M. Nakajima, M. Hangyo and C. L. Pan, Appl. Phys. lett. **83**, 1322 (2003).
15.   T. A. Liu, M. Tani, M. Nakajima, M. Hangyo, K. Sakai , S. Nakashima, and C. L. Pan, Optics Express, **12**, 2954 (2004).
16.   T, A. Liu, K. F, Huang, C.-L, Pan, Z. Liu, H.Ohtake, and N, Sarukura, Jpn. J. Appl. Phys. **38**, L1333 (1999).
17.   Z. Liu, S. Ono, H. Ohtake, N. Sarukura, T. A. Liu, K.-F. Huang and C. L. Pan, Jpn. J. Appl. Phys. **39**, L366 (2000).
18.   P. Gu, M. Tani, and K. Sakai, F. Chang and C. L. Pan, Jpn. J. Appl. Phys. **38**, L1246 (1999).
19.   T. R. Tsai, C. Y. Chen, C.-L. Pan, R.-P. Pan, and X.-C. Zhang, Appl. Opt., **42**, 2372 (2003)
20.   R. P. Pan, T. –R. Tsai, C. –Y. Chen, and C. L. Pan J. Biological Phys. **29**, 335 (2003).
21.   T.-R Tsai, C.-Y. Chen, R.-P. Pan, C.-L. Pan, and X.-C. Zhang, IEEE Microwave Wireless Comp. Lett. **14**, 77 (2004).
22.   C.-Y. Chen, T.-R Tsai, C.-L. Pan, R.-P. Pan, Appl. Phys. Lett. 83, 4497 (2003).